Analysis and Optimisation of Wind-Induced Vibration Control for High-Rise Chimney Structures

Zhao-Dong Xu, Jun-Tao Zhu and Deng-Xiang Wang

Key Laboratory of C&PC Structures of the Ministry of Education, Southeast University, Nanjing, China

Wind is a key factor when determining the safety of high-rise structures, such as buildings, chimneys, or towers. Using dampers to control wind-induced vibration is a safe, effective, and economical method for high-rise structures to employ. In this paper, viscoelastic dampers (VEDs) were used to reduce the dynamic responses of a 75-metre-high chimney. First, a simulation method for the stochastic wind field, based on the modified Fourier spectrum, was proposed. The method provided the accurate data of the wind velocity time history, which then simulated wind pressure through the use of a numerical wind tunnel. Then, the finite element model for the Madagascar chimney structure was built, and a wind-induced vibration analysis of the structure with and without VEDs was carried out under the simulated wind excitation. The optimisation – method, based on the genetic algorithm, was used to optimise the location of the VEDs. It was concluded that the accuracy of the modified Fourier spectrum method (MFSM) was greatly improved, when compared to the spectrum representation method of simulating the stochastic wind field. VEDs can effectively reduce the dynamic responses of chimney towers, especially for the displacement responses. In addition, the proposed optimisation method quickly determined the optimum positions and necessary quantities of VEDs to use, which yielded effective vibration mitigation.

1. INTRODUCTION

With the advancement of construction techniques, civil engineering structures have become larger, higher, and lighter. Some examples of such structures include high-rise buildings, skyscrapers, long-span space structures, and bridges. All such modern structures are extremely sensitive to wind excitation. As is well known, wind is a natural force with great destructive power. Damage due to excessive wind has become a serious problem lately, due to global warming, and has led to a loss of tens or hundreds of billion dollars per year to the global economy. Therefore, it is significant to study wind vibration responses and to take reasonable control measures when constructing high-rise structures.

Making accurate predictions of wind loads and their effects on high-rise structures is therefore a necessary step in the design process, and static analysis under wind loads is not suitable for structural design and the corresponding safety targets. Therefore, dynamic analysis of these structures under wind loads is becoming more and more significant. A time-domain analysis method is usually applied in dynamic analysis under wind loads, which provides evidence for structural design and fatigue analysis, but wind velocity time history around structures should be determined before time-domain dynamic analysis is tested. Subsequently, the wind velocity time history should be changed into wind pressure time history based on the wind pressure distribution characteristics on the structural surface.[1–3] Generally, wind velocity time history is generated according to wind velocity spectrums with special characteristics, such as the Davenport Spectrum, the Kaimal Spectrum, and the Harris Spectrum, which are summarized based on strong wind records. Such wind velocity spectrums are highly representative and accurate, which satisfy the demands of simulation of wind velocity time history and dynamic analysis. However, field measurements are not economic and lead to heavy workload, which limits wider application. Currently, the spectrum representation method[4] and the autoregressive method[5] are usually applied in the simulation of the stochastic wind field. The autoregressive method is based on a linear filtering technique: i.e., a white noise process with an average value of zero is passed through a filter, and a random process with a special spectrum is exported. The autoregressive method is efficient and requires little calculation, which leads to fast calculation speed. However, this method is less accurate when compared to the spectrum representation method. In fact, the precision of the spectrum representation method usually does not meet the calculation requirements. Moreover, the spectrum representation method has the drawback of a slow calculation speed. Therefore, the modified Fourier spectrum method (MFSM) has been introduced into the simulation of a stochastic wind field for the purpose of this paper. The phase information of a simulated point was determined by the cross power spectral density (CPSD) between the simulation and the adjacent points. Combined with the auto power spectral density (APSD) of the simulation points, an iterative modification for the Fourier spectrum was carried out. The wind velocity time history, with special time and space correlation, was then generated. Finally, Simulation of the wind field for a high-rise chimney was undertaken, to verify the effectiveness of the MFSM.

Another important point of research regards the process of taking measures to reduce the wind-induced vibration responses of high-rise structures. In 1972, Yao[6] first proposed the concept of structural control. The viscoelastic damper (VED) is the common passive control method. The main advantages of employing VEDs are to mitigate structural vibration most economically and effectively, while also achiev-

ing high reliability. The VED is acknowledged as one of the most efficient energy absorbing devices for building structures against dynamic loads such as earthquakes or wind.[7] Previous studies have shown that the efficiency of added VEDs can be greatly enhanced by applying properly sized dampers to the correct locations. For example, VEDs installed in a steel tower located in Pittsburgh, Pennsylvania, U.S.S., decreased the wind-induced vibration, and the dynamic responses of the tower were decreased by 40 % – 80 %.[8] 260 large VEDs were installed in the Columbia Center building in Seattle, Washington, U.S.A., in order to control the vibration induced by wind.[9]

According to analysis, the damping of the structure was increased from 0.8 % to 6.4 %, and the dynamic responses of the structure were also effectively reduced. Practical issues and solutions on the installation of VEDs in a high-rise building structure were reported.[10] A synthetic optimisation method was proposed to determine the optimal parameters and locations of dampers, using numerical analysis and a shaking table test of a reinforced concrete structure.[11] Because the VED played a significant role in reducing the structural vibration responses to wind or earthquakes, a study about vibration control of high-rise structures and location optimisation of VEDs, based on a Madagascar chimney structure, was conducted. The contributions of this study are: (1) the MFSM was firstly introduced for simulating the stochastic wind field, which can provide accurate wind velocity time history data to simulate the fluctuating wind pressure; and (2) the optimisation method, based on the genetic algorithm was proposed to find out the optimal location and quantity of VEDs required to effectively reduce dynamic responses of Madagascar chimney structures.

2. WIND LOAD SIMULATION

2.1. Theoretical Description

2.1.1. Fluctuating Wind Velocity Spectrum and the Space Coherence Function

Based on records, fluctuating wind can be simulated by a zero–mean, Gaussian, stationary, stochastic process. The wind power spectrum reflects the relationship between wind speed and frequency. At present, many types of wind velocity spectrums have been proposed, such as the Davenport spectrum, the Carmen spectrum, the Harris spectrum, the Simiu spectrum, and the Kaimal spectrum, among others. In this paper, the Kaimal spectrum was adopted, and its expression written as

$$\frac{nS(n)}{u_*^2} = \frac{200f}{(1+50f)^{5/3}}; \qquad (1)$$

where $S(n)$ represents the wind spectrum density, which is usually normalized in order to obtain the reduced spectrum $\frac{nS(n)}{u_*^2}$ of wind speed fluctuations. The product $nS(n)$ (known as the non-normalized spectrum) of the frequency n, in Hz, and the spectrum $S(n)$ was used so that the area between the two frequencies represented the variance contributed by that frequency interval. In general, the wind spectrum density was usually analysed against the normalized frequency $f = \frac{nz}{U(z)}$, known as the Monin (or similarity) coordinate, which is essentially the ratio of height to wavelength. $U(z)$ represents the mean wind speed at height z, and the so-called friction velocity u_* was a scaled velocity to represent the shear strength at the

boundary layer. This was calculated as $u_* = \frac{kU(Z)}{\ln(\frac{z}{z_0})}$, in which k is the Von Karman's constant and z_0 is the roughness length.

Space correlation exists in wind excitation to structures, which is a function regarding the distance between points in space, and can be expressed by the correlation coefficient in accordance with the Davenport form[12] as (2), where $\overline{v}_i$ and $\overline{v}_j$ are the mean wind velocity of point i and j, respectively; and C_x, C_y, C_z are the attenuation coefficients of the x, y, z directions, respectively.

2.1.2. Simulation of Fluctuating Wind Velocity

The MFSM is primarily used for simulating earthquake excitation. The basic idea of this method[13] can be described as a design response spectrum (i.e., a target response spectrum), which should be determined according to design parameters, such as seismic intensity and site classification. The power spectrum of the artificial seismic wave can be calculated approximately, according to the target response spectrum. The Fourier spectrum can then be obtained by a Fourier transformation from the calculated power spectrum. Then, the artificial seismic wave can be obtained by a Fourier transformation for the random phase and addition of the strength envelopes. Subsequently, the response spectrum of the artificial seismic wave may be calculated, and the previous Fourier spectrum should then be modified by the ratio of the target response spectrum to the response spectrum. Finally, the artificial seismic wave should be re-generated by the above-mentioned method.

Artificially-simulated seismic waves are usually generated on the base of the target design spectrum, but this method does not take the time and space correlation of multi-support excitation into consideration. For the simulation of the stochastic wind field, the wind velocity time history was also generated, according to the power spectrum. Therefore, this method of artificially-simulated seismic waves can be used to simulate the stochastic wind field if the method is modified appropriately and the time and space correlation of multi-support excitation is considered.

For the spectrum representation method,[14] the Cholesky decomposition must be undertaken for the power spectral density matrix $\mathbf{S}^0(\omega)$, in order to obtain $\mathbf{H}(\omega)$, which will be used to determine phase information. The Cholesky decomposition has low calculation efficiency, and decomposition cannot always be performed because of the singularity of $\mathbf{S}^0(\omega)$. In this paper, the phase information of a simulated point was determined by CPSD between this point and the adjacent point. Combined with APSD, the wind velocity time history was then simulated, and the Cholesky decomposition was therefore avoided. This process generated efficient results with excellent accuracy.

$\mathbf{S}^0(\omega)$ was the same for all simulation points; i.e., $S_{ii}^0(\omega) = S_{11}^0(\omega)(i = 1, 2, ..., m)$. The wind velocity time history of the first point was generated according to its APSD, $S_{11}^0(\omega)$). For example, the APSD of the second point, $S_{22}^0(\omega)$, was equal to $S_{11}^0(\omega)$, and the phase information, $\phi_2(\omega)$, was determined by the CPSDs $S_{21}^0(\omega)$ and $S_{22}^0(\omega)$. By the same means, the APSD of the ith point $S_{ii}^0(\omega)$ was also equal to $S_{11}^0(\omega)$, and the phase information $\phi_i(\omega)$ was determined by $S_{i,i-1}^0(\omega)$ and $S_{ii}^0(\omega)$. Supposing $L_{ii}(\omega) = \sqrt{S_{ii}^0(\omega)} = \sqrt{S_{11}^0(\omega)}$, the mod-

$$Coh(i,j,n) = exp\left\{\frac{-2n\sqrt{C_x^2(x_i-x_j)^2 + C_y^2(y_i-y_j)^2 + C_z^2(z_i-z_j)^2}}{\overline{v}_i + \overline{v}_j}\right\}. \qquad (2)$$

ified function of the phase can be expressed as

$$L_i(\omega) = \frac{S_{i,i-1}^0(\omega)}{L_{ii}(\omega)} = \frac{S_{i,i-1}^0(\omega)}{\sqrt{S_{11}^0(\omega)}}; \qquad (3)$$

and the phase can be expressed as

$$\phi_i(\omega) = \tan^{-1}\left\{\frac{Im\,[L_i(\omega)]}{Re\,[L_i(\omega)]}\right\}; \qquad (4)$$

where $Im\,[L_i(\omega)]$ and $Re\,[L_i(\omega)]$ are the imaginary part and the real part of $L_i(\omega)$, respectively. Consequently, the phase information matrix $\phi(\omega)$ was constructed as

$$\phi(\omega) = [\phi_1(\omega)\cdots\phi_i(\omega)\cdot\phi_m(\omega)]. \qquad (5)$$

The target power spectral density matrix was obtained from Eqs. (1) and (2). The Fourier spectrum $A_{ii}(\omega)$ was calculated as follows according to APSD (i.e. $S_{ii}(\omega)$):

$$A_{ii}(\omega) = \left(\frac{4 \times S_{ii}(\omega) \times 2\pi \times fs}{nfft}\right)^{\frac{1}{2}}; \qquad (6)$$

where fs is the sampling frequency of simulating the wind velocity time history, and $nfft$ is the number of points of the Fourier transformation.

$\phi_i(\omega)$ can be obtained by Eq. (4), and then the Fourier spectrum can be changed into a complex form combined with $\phi_i(\omega)$ as:

$$C_{ii}^k(\omega) = A_{ii}^k(\omega) \times e^{i\phi(\omega)}; \qquad (7)$$

where $i = \sqrt{-1}$. The inverse fast Fourier transformation was undertaken for $C(\omega)$, which was the combination of $C_{ii}(\omega)$. The wind velocity time history, $Y_i^k(t)$, was then generated based on the real part of the inverse fast Fourier transformation, resulting as:

$$y_i^k(t) = ifft\left(C_{ii}^k(\omega)\right); \qquad (8)$$

and

$$Y_i^k(t) = real\left(y_i^k(t)\right). \qquad (9)$$

The APSD of $Y_i(t)$ can be calculated by

$$S_{ii}^k(\omega) = psd\left(Y_i^k(t)\right). \qquad (10)$$

The new Fourier spectrum $A_{ii}^k(\omega)$ of $Y_i^k(t)$ can be calculated by

$$A_{ii}^k(\omega) = \left(\frac{4 \times S_{ii}^k(\omega) \times 2\pi \times fs}{nfft}\right)^{\frac{1}{2}}. \qquad (11)$$

Then, the previous Fourier spectrum $A_{ii}^k(\omega)$ should be modified by the ratio between $A_{ii}(\omega)$ and $A_{ii}^k(\omega)$ as:

$$A_{ii}^{k+1}(\omega) = A_{ii}^k(\omega) \times \frac{A_{ii}(\omega)}{A_{ii}^k(\omega)}. \qquad (12)$$

Finally, $A_{ii}^k(\omega)$ was Eq. (7) is substituted by $A_{ii}^{k+1}(\omega)$, and the wind velocity time history was obtained according to the given iteration times.
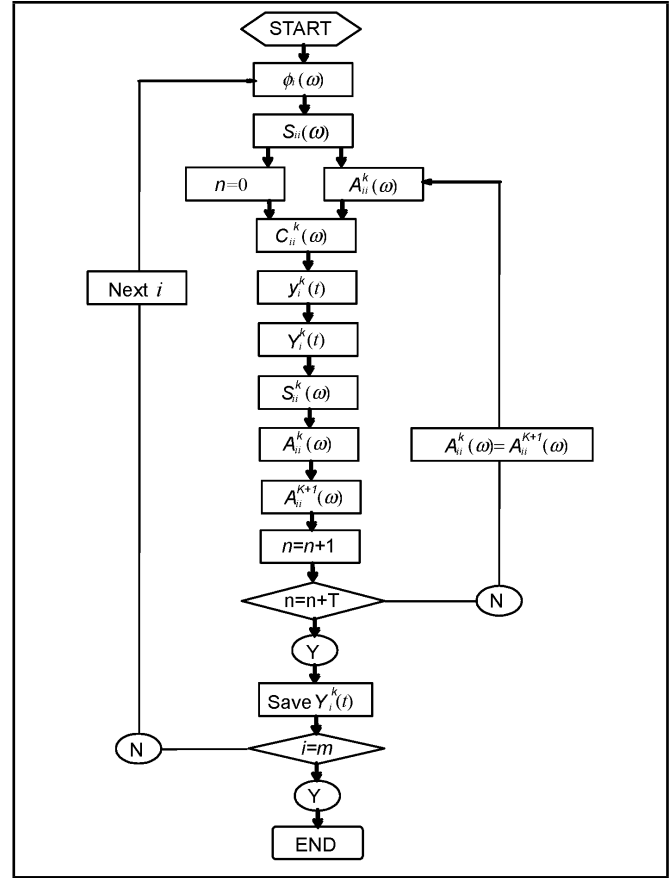
Figure 1: The calculation procedure of the MFSM.

The calculation process of the MFSM can be summarized as shown in Fig. 1. First, the target power spectral density $S_{ii}(\omega)$ was calculated by the previous $\phi_i(\omega)$, and then the phase deviation $\phi_i(\omega)$ was obtained by Eqs. (3) and (4), based on $S_{ii}(\omega)$. Second, the Fourier spectrum $A_{ii}(\omega)$ was estimated by Eq. (6), and then transformed to a complex form, $C(\omega)$, by Eq. (7). Finally, the inverse fast Fourier transformation was applied for $C(\omega)$, and the wind velocity time history, $Y_i^k(\omega)$, was generated based on the real part of the inverse fast Fourier transformation result. Then, $A_{ii}^k(\omega)$ in Eq. (7) is substituted for $A_{ii}^{k+1}(\omega)$ in Eq. (12). Next, refer to step two and start a new calculation. Iterative calculation was continued until the given time period T was completed, and thus the wind velocity time history was obtained.

2.1.3. Simulation of Fluctuating Wind Pressure Based on a Numerical Wind Tunnel

The numerical wind tunnel is a method to simulate wind fields based on computational fluid dynamics, which can accurately calculate the surface pressure distribution characteristics of structures. However, it cannot reflect the spectrum characteristics of fluctuating wind because of the use of the mean wind. This problem can be solved when taking fluctuating wind velocities, simulated by the MSFM, as the wind environment of the numerical wind tunnel. Therefore, the simulation results can both reflect the characteristics of wind pressure dis-
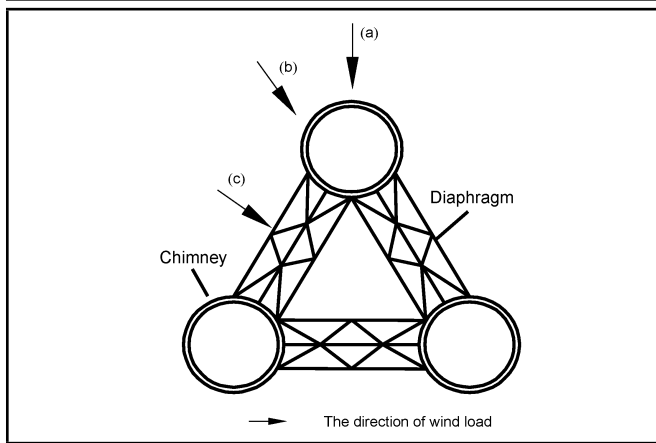
Figure 2: The structure plane diagram of Madagascar and the direction of the wind load.

tribution and the spectrum characteristics of fluctuating wind.

In this paper, the wind velocity time history, simulated by the MFSM, was applied for the boundary condition of the numerical wind tunnel. The wind pressure characteristics of the structure's surface were determined by using the user-defined function of the FLUENT software. The process can be summarized as

(1) Establishing the FLUENT model,

(2) Generating the wind velocity time history according to the inlet of the FLUENT model,

(3) Compiling the UDF program and substituting the wind velocity time history into the boundary condition,

(4) Setting other parameters of the FLUENT model,

(5) Calculating and taking record of the result, and

(6) Exporting and treating data to obtain stochastic wind pressure.

2.2. Wind Field Simulation of the Madagascar Chimney

2.2.1. Engineering Overview

The structure studied in this paper was a three tube chimney structure located in Madagascar. Considering the impact of tropical storms, the design wind velocity was $50\frac{m}{s}$. Converting this into basic wind pressure yielded $1.50\frac{kN}{m^2}$, and the landform category is B(GB50009-2001).[15] The structure plane diagram is shown in Fig. 2. The chimney plane with the pipe diameter of 3.2 m was an equilateral triangle, and the centre spacing was 7.0 m. The maximum width and height of the chimney was 10.2 m and 75 m, respectively. There were 11 diaphragm beams composed of steel truss sets on the elevation along the chimney height. The thickness of the wall of the chimney was 16 mm, where the corrosion-resistant weathering steel Q235NH was adopted. Its yield strength and ultimate strength were 216 MPa and 285 MPa, respectively.

The structural wind shape coefficient was mainly decided in accordance with the chimney pipe. The effect of the diaphragm beam was properly considered, because of its smaller
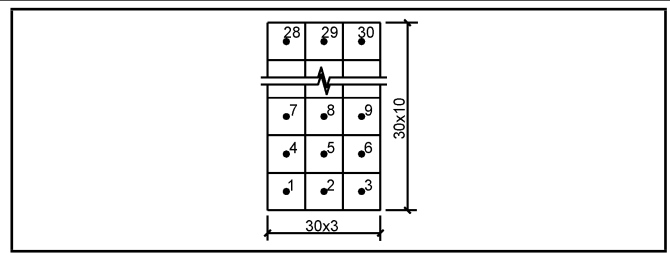
Figure 3: The points' distribution at the numerical wind tunnel inlet.

projected area on the windward side. As wind direction is arbitrary in practice, three representative directions were selected, as shown in Fig. 2.

A closed rectangular shape was used to represent the calculation model of the numerical wind tunnel. The dimensions of the numerical wind tunnel were $90 \times 300 \times 600$ m, the mesh size of which was about $10m$. The blocking probability was 2.6%. The distance between the windward sides of the chimney model to the inlet boundary was $\frac{L}{3}$, and the leeward side of the model to the tunnel exit was $\frac{2L}{3}$.

According to the different wind directions, the numerical wind tunnel models were established, as shown in Fig. 2. The mesh accuracy of these models (the different direction of wind load (a), (b) and (c)) were the same – i.e., the mesh size for the surfaces was 0.1 m, and the mesh size for the edges was 0.01 m.

2.2.2. Wind Velocity Simulation

The wind velocity time history simulation of the wind tunnel inlet was undertaken, which was based on the size of the wind tunnel inlet (90×300 m) and the coherence characteristics of the wind field. The design wind velocity was $50\frac{m}{s}$, and the landform category was B. In the numerical simulation, the Kaimal spectrum was adopted as the target spectrum, and the correlation function was expressed as the Davenport form. The horizontal and vertical attenuation coefficient of the wind tunnel section were $C_y = 8$ and $C_z = 7$, respectively. The upper limit frequency of the simulated wind velocity time history was 2 Hz, the time sampling frequency was 4 Hz, and the total sampling time was 1000 s. The inlet area was divided into 30 squares with the size of 30×30 m, which were chosen to fit the size of the wind tunnel inlet; therefore, a total of 30 points were used and each point represented a region of 30×30 m, as shown in Fig. 3.

Taking one point of these points in Figures 3 for example, the wind velocity time history and the APSD of fluctuating the wind of point five are displayed in Fig. 4. It can be seen from Fig. 4 that the APSD of the simulated wind velocity time history fit well with the target power spectrum density, and the higher accuracy of the simulation can be achieved when taking the wind velocity time history, obtained by the MFSM as an input of the numerical wind tunnel. Fig. 5 shows the CPSD of the wind velocity time history between the points two and five. As shown in the figure, the CPSD of the wind velocity time history obtained by the MFSM fit well within the target spectrum.

(a) The wind velocity time history   (b) The APSD of wind velocity at point 5
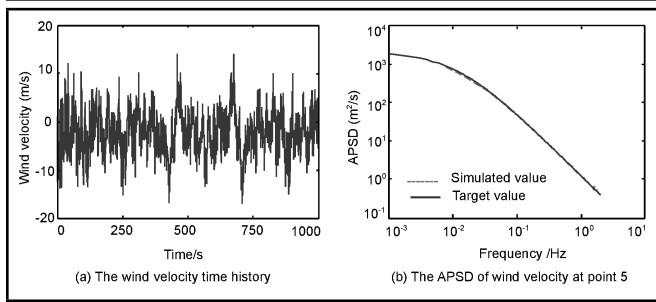
Figure 4: The wind velocity time history and its APSD of point 5, simulated by the MFSM.
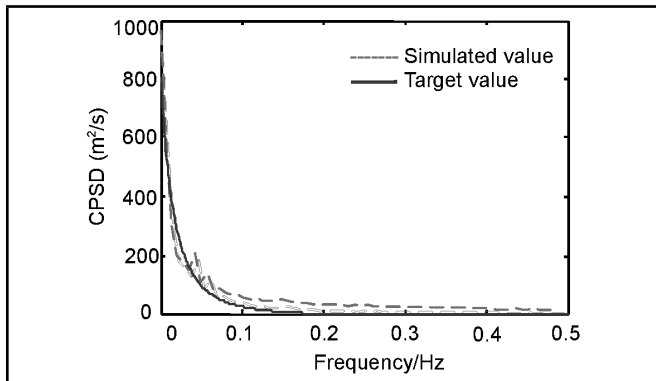
Figure 5: The CPSD of points 2 and 5, as simulated by the MFSM.

2.2.3. Wind Pressure Simulation

The large eddy simulation model was used as the turbulent model in this example, and the separation implicit solver was used for the calculation. The function of unsteady time was selected for calculating time, and the second-order implicit equation was used as the time equation. The time step was 0.25 s, the same as the wind velocity, and the total time was 1000 s. The SIMPLE algorithm and the standard form were used as the pressure-velocity equation and pressure algorithm, respectively, and the Quick form is used as the algorithm of the momentum and the energy equations. Convergence precision was defaulted by the software, of which the energy equation was 10^{-6} and the others were 10^{-3}. Additionally, the Reynolds number and Navier-Stokes equations were automatically considered by the FLUENT software when calculating the wind pressure. The boundary conditions used in this model mainly included the inlet boundary and outlet boundary. The velocity-inlet boundary condition and the outflow form boundary were separately adopted for the inlet boundary condition and outlet boundary condition of this calculated model. In addition, the slip wall boundary was adopted for other boundary conditions in the calculation region, such as the surface of the calculated model.

In order to compare the characteristics of fluctuating wind pressure and provide a basis for structural analysis, the fluctuating wind pressure of some critical points was monitored. Based on the structural features, each chimney pipe was divided into 88 planes, and each monitor point was located at the centre of each plane. There were a total of 176, 264, and 176 points selected to monitor for models (a), (b), and (c), respectively, as seen in Fig. 6. In order to compare these more easily, the monitor point was representatively selected according to
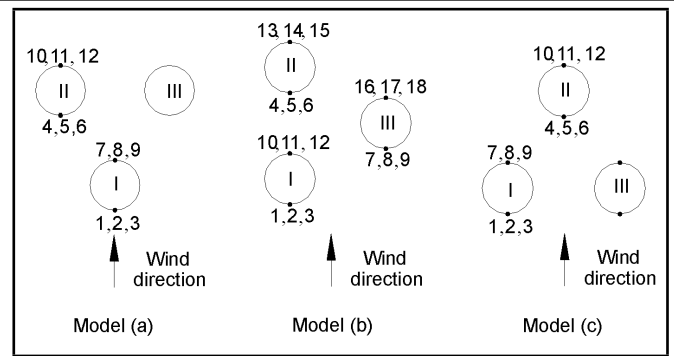
Figure 6: The monitoring points layout.

(a) The wind pressure time history   (b) The APSD of wind pressure at point 2
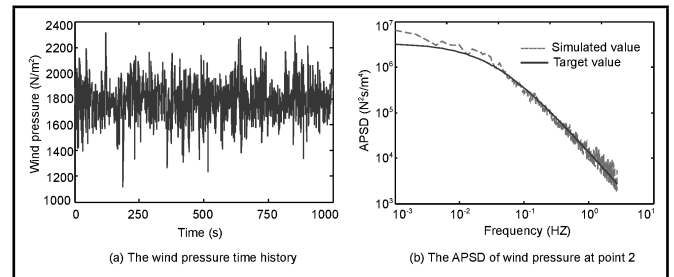
Figure 7: The wind pressure time history and its APSD of point 2 in Model (a).

the wind pressure characteristics of the structure surface. As seen in Fig. 6, there were 12 points selected in model (a). The locations of points 1, 2, and 3 were the centre of the windward side and their heights were 15 m, 45 m, and 75 m, respectively. The locations of the other points in model (a) were the same as those of points 1, 2, and 3. For model (c), the number of monitor points was same as in model (a). However, 6 monitor points were required to be chosen on each chimney pipe in model (b), because of the asymmetrical location of the three chimney pipes.

For model (a), the points 2 and 8 on pipe I and the points 6 and 11 on pipe II were selected to compare the wind pressure and the spectrum density. Fig. 7 shows the wind pressure time history, WPTH, and its APSD of point 2 (with a height of 45 m). As can be seen in Fig. 7, the APSD and the target spectrum of the fluctuating wind pressure of point 2, in the intermediate frequency part, were in good agreement. However, there was a slight deviation in the low frequency (less than 0.01 Hz) and the high frequency (more than 0.5 Hz) parts. Similar results were obtained at points 1 and 3. In terms of results, the simulation accuracy of the wind pressure simulated by FLUENT was good.

Fig. 8 shows the WPTH and the APSD of the point 6 (the height is 75 m). It can be seen from the figure that the APSD and the target spectrum of the fluctuating wind pressure of point 6 are in good agreement, but there was larger deviation in the lower frequency (less than 0.02 Hz) part. Additionally, the simulation accuracy of the APSD of point 6 was lower than that of the the point 2. Considering the coupling effect of the wind and the structure, the wind field characteristics of chimney pipe II were influenced by pipe I, which was because chimney pipe I occludes chimney pipe II. Similarly, the APSD and the target spectrum of the fluctuating wind pressure of point 8 (of height 45 m) were in good agreement in the intermediate frequency part, but there was larger deviation in the low frequency (less
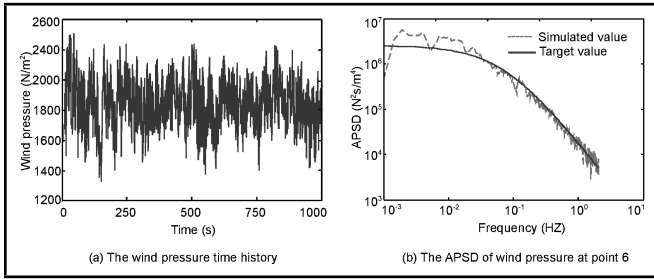
Figure 8: The wind pressure time history and its APSD of point 6 in Model (a).
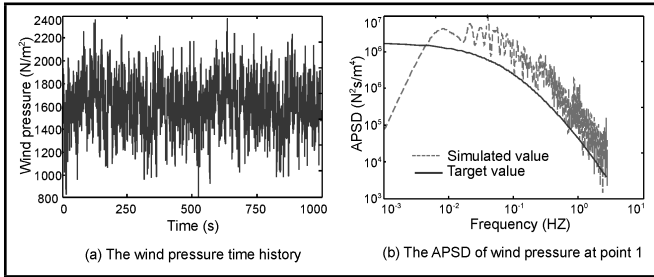
Figure 9: The wind pressure time history and its APSD of point 1 in Model (a).

than 0.02 Hz) and the high frequency (more than 0.5 Hz) part. Furthermore, the simulation accuracy of point 8 was obviously lower than that of point 2, and a similar result was obtained for point 11. This was because points 8 and 11 were located on the lee side of the structure, where the coupling effect of the wind and the structure were more obvious.

Fig. 9 shows the WPTH and the APSD of point 1 of model (a), which was simulated by the harmonic synthesis method. It can be seen from the figure that there was a large deviation between the APSD of the wind pressure time history and the target values, especially in the low and high frequency part. On the whole,the simulation accuracy of the harmonic synthesis method was less accurate than that of the MFSM.

In order to comprehensively study the characteristics of fluctuating wind by numerical wind tunnel simulation, the cross power spectrum characteristics were also analysed. The cross power spectrums of the wind pressure between points 1 and 2 in model (a) were based on the MFSM and the harmonic synthesis method of numerical wind tunnel simulation. The simulation results of the two methods and the target value were a close match, but the precision of the simulation result was not ideal. The simulation precision of the MFSM was slightly worse than that of the harmonic synthesis method. Above all, the precision of the numerical simulation of the wind pressure tunnel in cross power spectrum needs to be improved. For models (b) and (c), the same conclusion was obtained as in the study of model (a).

It can be concluded from the above analysis that the MFSM can accurately simulate the fluctuating wind velocity, due to the fact that the auto power spectrum and the target spectrum were almost identical. Additionally, the precision and efficiency of the MFSM was greatly improved compared to the traditional harmonic synthesis method. The power spectrum and the target spectrum were in accord at the intermediate frequency part, as well. However, there was a slight difference in the low and high frequency parts for the wind pressure simulation because of the use of the numerical wind tunnel when
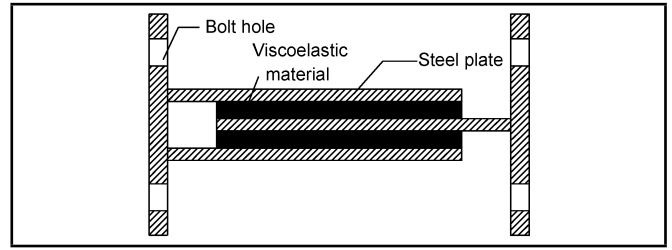
Figure 10: The structure diagram of the VED.

the input was adopted as the fluctuating wind velocity was obtained by the MFSM.

3. WIND VIBRATION CONTROL AND OPTIMISATION ANALYSIS

3.1. The Working Principle and Mathematical Model of the VED

The dynamic equation of the structure incorporated with the VEDs can be expressed as follows in (13), where $[M]$, $[C]$, and $[K]$ are respectively the structural quality, damping, and stiffness matrices; $[C_d]$ and $[K_d]$ are the VED's damping and stiffness matrices, respectively; $\{x\}$, $\{\dot{x}\}$, and $\{\ddot{x}\}$ are the displacement vector, velocity vector and acceleration vector of the structure, respectively; and $\{P(t)\}$ is the fluctuating wind load vector of the structure. $\{F(t)\}$ represents the control force vector of the structure, and $[H]$ is the position matrix of the structure control forces. It can be seen from the dynamic equation that the dynamic characteristics of the structure will change because of the contribution of the additional stiffness, K_d, and the additional damping, C_d, provided by the VED.

The commonly used VED, as shown in Fig. 10, is made up of three steel plates clamping two VE layers. When VEDs are incorporated into structures, the control forces provided by VEDs are usually written as:

$$F_d = c_d \dot{\Delta} + k_d \Delta;　(14)$$

where F_d represents the forces produced by the VED, Δ and $\dot{\Delta}$ are the displacements and velocities produced in the VED, and c_d and k_d are the equivalent damping and stiffness. These can be written as:

$$k_d = \frac{n_v G_1 A_v}{h_v};　(15)$$

and

$$c_d = \frac{n_v G_1 \eta A_v}{\omega h_v};　(16)$$

where η is the loss factor ($\eta = \frac{G_2}{G_1}$), G_1 and G_2 are the storage modulus and the loss modulus for the VE material in dampers, n_v is the number of VE layers in each damper, A_v and h_v are the shear area and thickness of each VE layer, and ω is the excitation frequency. As shown, when a VED is designed and n_v, A_v, and h_v are determined, the key problem is determining the storage modulus G_1 and the loss factor η. Both parameters are affected by environmental temperature and excitation frequency.

In order to depict these effects, some mathematical models were proposed. The main models included the Kelvin model, the Maxwell model, the standard linear solid model, the complex stiffness model, the four parameters model, and the finite element model.[16–18] Among these mathematical models,

$$[M]\{\ddot{x}\} + ([C] + [C_d])\{\dot{x}\} + ([K] + [K_d])\{x\} = \{P(t)\} - [H]\{F(t)\}. \tag{13}$$

only the finite element model can simulate temperature and frequency effects simultaneously, seven though the model is very complex. Herein, based on the temperature-frequency equivalent principle and the standard linear solid model, Xu[19] proposed the equivalent standard solid model, which can reflect the effect of temperature and frequency on the performance of the VED. In this model, the key contribution was the simultaneous consideration of the effects of temperature and frequency on the shear modulus G_1 and the loss factor η of viscoelastic materials. When the temperature is in the range of T_g (the glass transition temperature) to $T_g + 100°$ C, in most viscoelastic materials the relationship between the temperature and frequency is equivalent;, i.e., the impact of low temperature is equivalent to that of high frequency, and the impact of high temperature is equivalent to that of low frequency. If the effects of temperature and frequency on viscoelastic material properties are taken into account, there will be

$$\left.\begin{array}{c} G_1 = \dfrac{q_0 + p_1 q_1 \alpha_T^c \omega^c}{1 + p_1^2 \alpha_T^c \omega^c} \\[2mm] \eta = \dfrac{(q_1 - p_1 q_0)\alpha_T^d \omega^d}{q_0 + p_1 q_1 \alpha_T^{2d} \omega^{2d}} \end{array}\right\}; \tag{17}$$

where $\alpha_T = 10^{\frac{-12(T-T_0)}{[525+(T-T_0)]}}$ is the temperature conversion factor which is a function of temperature T. The indexes c and d are determined by trial. The working temperature and frequency range of VEDs are usually $-30°C \leq T \leq 60°C$ and 0.1 Hz$\leq \omega \leq 10$ Hz.

The equivalent standard solid model can reflect the creep characteristic and slight relaxation characteristic of the VED, and can accurately reflect the variation of the storage modulus and the loss factor with temperature and frequency. The VEDs developed by Southeast University and Damper Technology Co., Ltd., in Changzhou, were used in this example to reduce the wind induced responses. The storage modulus G_1, the loss modulus G_2 and the loss factor η of viscoelastic material in the VED, respectively, were $3.75 \times 10^3 \frac{kN}{m^2}$, $2.25 \times 10^3 \frac{kN}{m^2}$, and 0.6.

3.2. Dynamic Response of the Chimney Tower Structure and Optimisation Analysis

3.2.1. Analysis of Wind Vibration Responses

The finite element model of the Madagascar chimney structure described in Section 2.2.1 was considered. Chimney tubes and diaphragm beams were simulated by spatial beam elements, and each VED were simulated by one spring element parallel with a viscous element. The equivalent stiffness of the spring element and the damping of the viscous element were determined by Eqs. (15)–(17). The calculated equivalent stiffness and damping for the designed VEDs were $13.93 \frac{kN}{mm}$ and $1.509 \frac{kN·s}{mm}$, respectively. The stroke and the corresponding maximum damping force of this kind of VED were 40 mm and 10 t, respectively. The built model is shown in Fig. 11 (a), and the dampers instalment style and elements number can be seen in Fig. 11 (b). The connections between members were considered as rigid nodes. Because the bar element cannot be im-
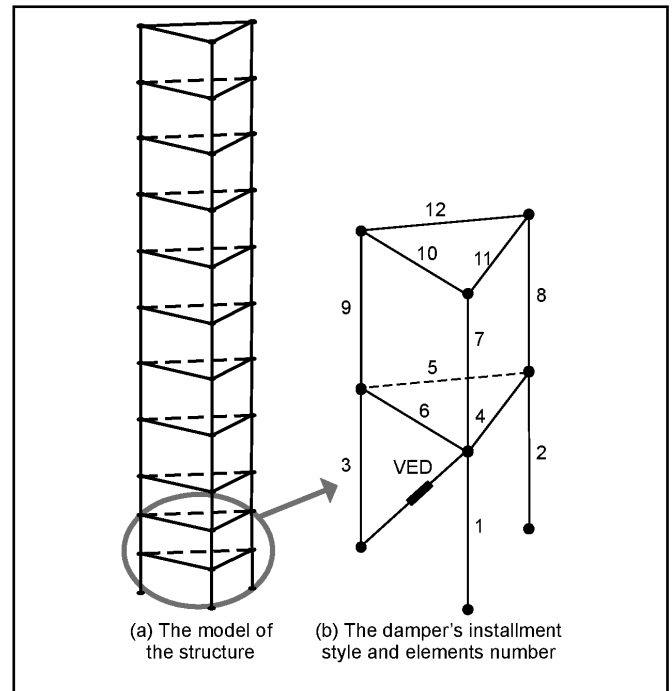
Figure 11: The finite element model for the Madagascar chimney structure.

posed on surface loads, the wind pressure acting on the structure was converted into the concentrated loads applied on all nodes. The fluctuating wind pressure time history of the different parts of structure surface was simulated by the method described in Section 2.

In solving Eq. (13), the Rayleigh damping matrix was adopted, the Wilson-θ method was chosen as the time history solution method at $\theta = 1.4$, and the sample time step was 0.25 s.

3.2.2. Optimisation for VED Location

In fact, the structure wind-induced responses were greatly affected by the locations and quantities of VEDs; therefore, one key problem was how to optimise the locations and quantities of VEDs in structures. In this paper, the locations of VEDs in Madagascar chimneys were optimised by using the genetic algorithm method, which is an optimisation algorithm based on the natural genetic mechanisms of biological evolution.[20]

The selection of the objective function is the key to optimizing VED location. For the chimney tower structure in this example, the structural top displacement was as the control objective function as:

$$max(x_n(t)) - \frac{h}{100} \leq \varepsilon; \tag{18}$$

where $x_n(t)$ was the displacement response time history of the top floor, ε was a smaller limited value, and 50 mm was adopted as the smaller limited value. During the process of optimisation, a supposed $0 \sim 1$ VED could be installed in each diagram brace in the plane frames, so the constraint condition for the damping contributed to each plane frame can be written as

$$0 \leq C \leq C_e; \tag{19}$$

where C_e is the equivalent damping of the VED used in the paper.

Optimising the locations and quantities of VEDs in structures can be summarized as follows. First, the information of the member, the materials, and the loads must be entered into the analysis model. Second, the control objective function, shown as Eq. (18) and the constraint condition, shown as Eq. (19) should be inputted, and the optimal damping of each location calculated using the genetic algorithm. Then, each VED needs to be installed in the structure in the descending order of contribution damping obtained by the genetic algorithm. The wind vibration responses of the structure must then be calculated, and a comparison of the maximum value of the structural top displacement with the vertex displacement limit value should be conducted next. If the maximum vertex displacement response exceeds the limit value, the next damper should be added in the place with the maximum contribution damping, among the places without dampers, till the maximum vertex displacement response is less than the limit value. According to the code for the design of high-rise structures, GB50135-2006[21] and the code for design of chimneys, GB50051-2002,[22] the maximum vertex displacement response of high-rise structure under wind or seismic excitations should be less than $\frac{1}{100}$ of the structure height. The height of the structure used in this study was 75 m; therefore, the limit of vertex displacement was calculated to be 750 mm. The programs were made in MATLAB software, in accordance with the above idea. The optimisation results showed that 18 VEDs were required to be installed in the structure, and the locations of these dampers can be seen in Fig. 12a.

3.2.3. Results Comparison

In order to verify the effectiveness of the optimisation results, the dynamic responses between the structures with the optimal instalment and the random instalment of dampers were compared. The random instalment, in which VEDs were installed in the upper part of the chimney with the larger storey shifts, is shown in Fig. 12b. The sum of the dampers was also 18.

The natural periods of structures with and without dampers were calculated by the software SAP2000 and the self-compiling programs in MATLAB. The calculated results are listed in Table 1. It can be seen in Table 1 that all of the mode periods for the structure with VEDs were smaller than those of the original structure, which indicates that the structure achieved rigidity when the VEDs were added. This is because the VEDs provided additional stiffness for the structure, as well as damping. In addition, the results calculated by MATLAB were almost the same as those determined by SAP2000. This demonstrates that the self-compiling program correctly calculated results, which can then be used to analyse the structure vibration responses under wind excitation.

Considering that the wind pressure time history was longer and the data more intensive, the $0 - 200$ s time history curves were adopted for the purpose of easily comparing the control effect. The time history of the vertex displacement responses of the structure with dampers and without dampers, under the wind excitation in Model (a) are shown in Fig. 13a. It can be seen in Fig. 13a that the vertex displacement responses of the structure incorporated with VEDs were effectively re-
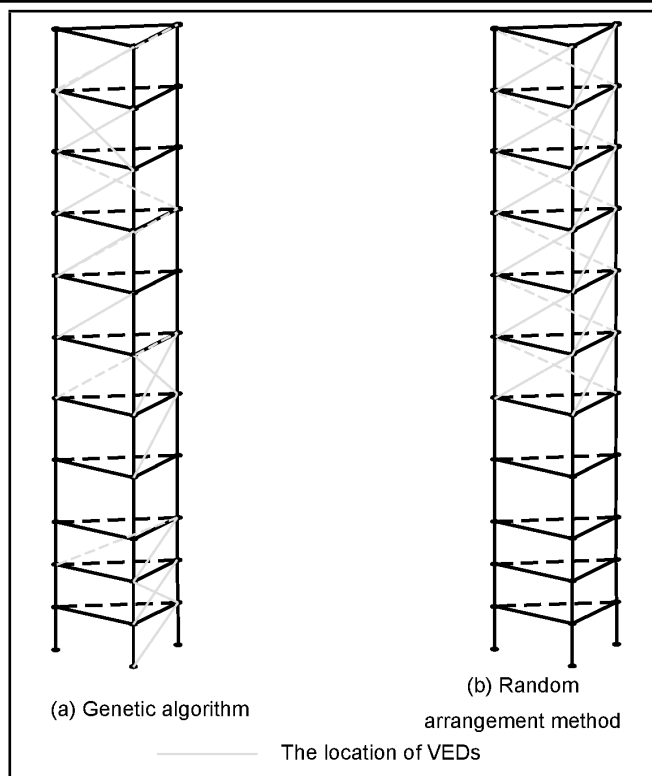
Figure 12: The arrangement diagram of the VEDs.

duced. The figure also shows that the displacement responses of the structure with the optimal instalment of dampers were reduced more obviously than those with the random instalment of dampers. The vertex displacement amplitude of the uncontrolled structure under the wind excitation reached 776 mm, which was greater than the limit value 750 mm. The vertex displacement amplitude of the optimally-controlled structure was 495 mm, and that of the randomly controlled structure was 583 mm. The maximum displacement responses were reduced by 36.2% and 24.9%, respectively, compared to that of the uncontrolled structure. The time history of the vertex acceleration responses of the three kinds of structures are shown in Fig. 13b. As the figure shows, conclusions similar to those mentioned above were obtained; however, the control effect of the displacement responses was better than that of the acceleration responses. Similar analysis results were also obtained for Model (b) and Model (c).

In order to effectively show the vibration mitigation ability of VEDs for the chimney, the wind vibration responses at 45 m of height were also studied. Fig. 14a and Fig. 14b show the time history curves of the displacement and acceleration responses of the point at 45 m height, with and without dampers, under the wind excitation in Model (a). The same vibration mitigation effect as that of the chimney's vertex was found. The maximum displacement responses of different heights of the controlled and uncontrolled structures under fluctuating wind pressure are shown in Fig. 15. It can be seen that the displacement responses of the structure were effectively reduced when VEDs were incorporated into the structure. It was also shown that the optimally-controlled structure had better control effect than the randomly controlled structure did.

Table 1: The natural periods of the structure.

Modes order	SAP200 simulation			Matlab simulation	
	The original structure	Genetic Algorithm	Random arrangement method	The original structure	Genetic Algorithm
1	1.065	0.899	0.848	1.090	0.886
2	0.977	0.789	0.779	0.797	0.797
3	0.558	0.543	0.544	0.613	0.561
4	0.544	0.457	0.512	0.380	0.497
5	0.302	0.280	0.277	0.339	0.380
6	0.289	0.269	0.267	0.289	0.339
7	0.241	0.220	0.211	0.235	0.303
8	0.239	0.212	0.202	0.209	0.263
9	0.232	0.211	0.202	0.189	0.254
10	0.211	0.187	0.194	0.182	0.236
11	0.194	0.181	0.190	0.177	0.207
12	0.189	0.176	0.183	0.169	0.189
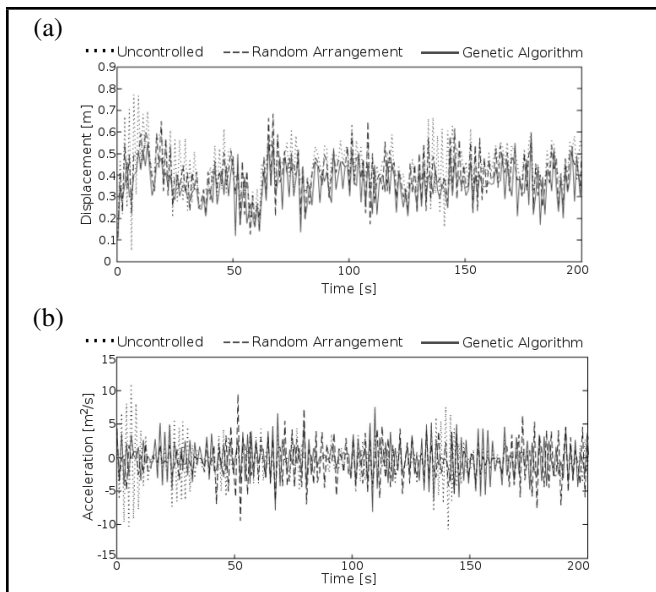
Figure 13: The vertex structural responses of Model (a); a) The time history curve of displacement, b) The time history curve of acceleration
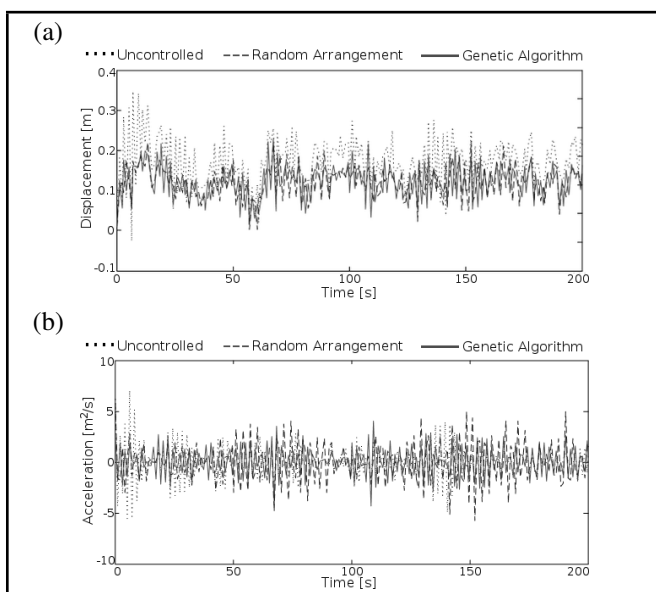
Figure 14: The midpoint structural responses of Model (a); a) The time history curve of displacement, b) The time history curve of acceleration
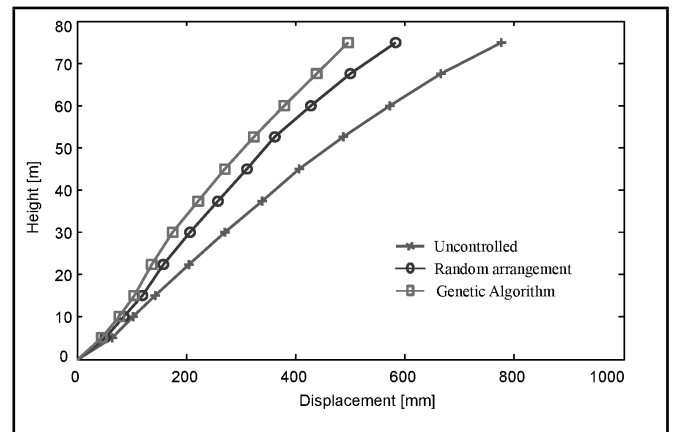
Figure 15: The envelope diagram of the horizontal displacement responses of the chimney.

4. CONCLUSIONS

In this paper, the MFSM was introduced to simulate the stochastic wind field. Under the simulated wind excitation, the wind response analysis of a Madagascar chimney structure with and without VEDs was compared. The locations and quantities of the VEDs required were determined by the genetic algorithm. The following conclusions can be obtained from the above analysis:

(1) The MFSM had excellent correlation between the APSD of the simulated wind velocity time history and the target power spectral density, and the simulation accuracy was greatly improved as compared to the harmonic synthesis method.

(2) The APSD of fluctuating wind pressure, simulated by the numerical wind tunnel, were in good agreement with the target spectrum in the middle frequencies, while a little poor in the high and low frequencies. On the whole, it can accurately reflect the characteristics of wind pressure distribution and basically retain the frequency spectrum characteristics of wind pressure. Therefore, it is reasonable to simulate the wind excitation for structural wind vibration analysis using the MFSM.

(3) The dynamic responses of the Madagascar chimney, especially the displacement responses, were effectively reduced when VEDs were installed in the structure.

(4) The proposed optimisation algorithm can quickly find the optimal location and quantities of VEDs, which have a better control effect than the random instalment method does.

ACKNOWLEDGMENTS

REFERENCES

[1] Lazzari M., Vitaliani R., Majowiecki M., et al. Dynamic behavior of a tensegrity system subjected to follower wind loading. Computers and Structures, **81**(22), 2199–2217, (2003).

[2] Mazanoglu K., Yesilyurt I. and Sabuncu M. Vibration analysis of multiple-cracked non-uniform beams. Journal of Sound and Vibration and Control, **320**(4), 977–989, (2009).

[3] Moustafa A. and Takewak I. Use of probabilistic and deterministic measures to identify unfavorable earthquake records. Journal of Zhejiang University-SCIENCE A (Applied Physics & Engineering), **10**(5), 619–634, (2009).

[4] Shinozuka M., Yun C. B. and Seya H. Stochastic methods in wind engineering. Wind Engineering and Aerodynamics, **36**(2), 829–843, (1990).

[5] Samaras E., Shinozuka M. and Tsurui A. ARMA representation of random processes. Journal of Engineering Mechanics, **111**(3), 449–461, (1985).

[6] Yao L. N. Concept of Structural Control. Journal of the Structural Division, ASCE, **98**(7), 1567–1574, (1972).

[7] Xu Z. D., Wang D. X. and Shi C. F. Model, tests and application design for viscoelastic dampers. Journal of Vibration and Control, **17**(9), 1359–1370, (2010).

[8] Soong T. T. and Dargush G. E. Passive energy dissipation systems in structural engineering. England (Chichester), John Wiley & Sons, 1651–1671, (1997).

[9] Mahmoodi P. and Keel C. J. Performance of structure dampers for the Columbia Center Building. New York: In Building Motion in World, ASCE, 83–106, (1986).

[10] Ahn S. K., Min K. W., Park J. H., et al. Practical issues and solutions on installation of viscoelastic dampers in a 46-storey reinforced concrete building structure. Structural Design of Tall and Special Buildings, **17**(1), 231–243, (2008).

[11] Xu Z. D., Zhao H. T. and Li A. Q. Optimal analysis and experimental study on structures with viscoelastic dampers. Journal of Sound and Vibration, **273**(3), 607–618, (2004).

[12] Davenport A. G. The dependence of wind load upon meteorological parameters. In: Proceedings of the International Research Seminar on Wind Effects on Buildings and structures (Toronto, 1968). Toronto: University of Toronto Press, (1968).

[13] Wang J. and Hu X. Application of Matlab in treatment of vibration signal. Beijing: China Water Power Press, (2006). (In Chinese)

[14] Xu Z. D., Wang D. X. and Wu K. Y. Simulation of stochastic wind field for large complex structures based on modified Fourier spectrum. J Zhejiang Univ-Sci A (Appl Phys & Eng), **12**(3), 238–246 (2011).

[15] Load code for the design of building structures (GB5009-2001). National Standards of P.R.C, (2001). (In Chinese)

[16] Markis N. Complex-parameter Kelvin model for elastic foundation. Earthquake Engineering and Structural Dynamics, **23**, 251–264, (1994).

[17] Kasia K., Munshi J. A., Lai M. L., et al. Viscoelastic damper hysteretic model: theory, Experiment and application. Proceedings of ATC 17-1 on Seismic Isolation, Energy Dissipation and Active Control, 2, 521–532, (1993).

[18] Tsai C. S. Temperature effect of viscoelastic dampers during earthquakes. Journal of Structural Engineering, ASCE, **120**(2), 394–409, (1994).

[19] Xu Z. D. Earthquake mitigation study on viscoelastic dampers for reinforced concrete structures. Journal of Vibration and Control, **13**(1), 29–45, (2007).

[20] Kwon Y. D., Kwon S. B., Jin S. B., et al. Convergence enhanced genetic algorithm with successive zooming method for solving continuous optimization problems. Computers and Structures, **81**(1), 1715–1725, (2003).

[21] Code for design of high-rising structures (GB50135-2006). National Standards of P.R.C, (2007). (In Chinese)

[22] Code for design of chimneys (GB50051-2002). National Standards of P.R.C, (2003). (In Chinese)